ISIJ International, Vol. 32 (1992), No. 3, pp. 440–449

Application of Mathematical Modelling to Hot Rolling and Controlled Cooling of Wire Rods and Bars

Ettore ANELLI

Department of Structural Steel Metallurgy, CENTRO SVILUPPO MATERIALI, P.O. Box 10747 Roma-Eur, Italy.

(*Received on September 2, 1991; accepted in final form on December 20, 1991*)

A set of integrated mathematical models for simulating hot rolling and controlled cooling of wire rods and bars has been developed through extensive laboratory research work and validation against carefully monitored results from industrial mills.

Experimental tests have been carried out on C–Mn and eutectoid steels selected as representative of the various applications of wire rods and bars.

Static and dynamic recrystallization of austenite, fraction of transformed austenite, final microstructures and mechanical properties are all calculated by modelling physical phenomena and using quantitative relationships between the microstructural and kinetic parameters and the process variables, *i.e.* strain, strain rate, temperature and time.

The models have been applied to predict the microstructure evolution during hot rolling and to investigate the effect of working conditions and recrystallization mechanisms on the formation of heterogeneous austenitic microstructures.

The effects of the cooling pattern on the temperature profile and the austenite phase transformation have also been studied to prevent: coarse pearlite and martensite formation at the centre of wire rods which have cores enriched in C and Mn; surface hardening of bars when water tube cooling systems are used to control the temperature at the cooling beds.

The models provide an important insight into the process that is beneficial to enhance the quality of long products.

KEY WORDS: mathematical modelling; hot rolling; controlled cooling; wire rod; bar; recrystallization kinetics; grain size evolution; phase transformation; mechanical properties; C–Mn and eutectoid steels; stored strain; hot torsion testing.

1. Introduction

A comprehensive steel rolling model should make accurate predictions of the effects of process variables on temperature distribution, microstructural evolution and their consequent effects on product properties. Considerable research has been devoted to computer modelling of hot rolling, including both thermomechanical and metallurgical aspects. The specific advances made in this field have been recently discussed during two international conferences.[1,2]

The work at CENTRO SVILUPPO MATERIALI (CSM) was initially concentrated on the development of microstructure and hot strength models for plate rolling of C–Mn and microalloyed steels.[3,4] The constitutive relations for microstructure evolution prediction were coupled with temperature and deformation models to optimize rolling schedules and improve rolling force prediction at ILVA's plate mill No.2 (ILVA is the major Italian steelmaking company), Taranto Steel Works. Both finite difference computing method (FDCM)[3,4] and finite element method (FEM)[5,6] were employed to model strain and temperature evolution.

This work summarises the extension of the thermomechanical and microstructural modelling to bar and wire rod rolling mills, where the very high stock speed and short interpass times, especially in the final stage of rolling, favours strain accumulation. Furthermore the high temperature gradients across the section, increased by the introduction of additional water cooling systems, lead to a microstructural gradient along the rod diameter.

In the paper, a set of models specifically designed to predict the thermal and microstructural evolution of C–Mn steel long products is outlined and their application to improve the quality of the final products is discussed.

2. Experimental Work

Experimental tests and rolling trials have been carried out on C–Mn and eutectoid steels for bars and wire rods (**Table 1**) in order to develop the models through laboratory research work and validation against carefully monitored results from industrial mills.

2.1. Laboratory Tests

Specimens taken from billets have been austenitized

Table 1. Chemical composition of steels (wt%).

Steel	Use	Chemical composition (%)						
		C	Mn	Si	Cr	B	Ti	Al
ES17	Welding wire	0.10	1.70	0.85	0.04	—	—	<0.005
QC29B	Fasteners	0.30	0.92	0.30	0.14	0.0024	0.05	0.025
IC43	Forging	0.40	0.70	0.25	0.15	—	—	0.03
FP69	Steel cord	0.71	0.66	0.24	0.03	—	—	<0.005
FF82	Ropes and	0.85	0.62	0.25	0.03	—	—	0.03
FF82K	Prestressed concrete	0.82	0.74	0.21	0.24	—	—	0.01

at temperatures ranging from 900 to 1 250°C for 2, 15 and 120 min and subsequently water quenched in order to define empirical grain growth laws.

Hot torsion tests have been performed on specimens having different austenitic grain sizes ($d_\gamma = 20$–$440\ \mu m$), varying both the deformation temperature ($T = 900$–1 150°C) and the amount of strain ($\varepsilon = 0.21$–0.64), in order to quantify the effect of the main metallurgical and process parameters on the softening kinetics and relevant structural modifications. The methodology developed by IRSID[7] and based on the performance of double hot torsion tests has been adopted for analyzing recrystallization kinetics. The size of the recrystallized austenitic grain has been measured by metallographic methods on specimens quenched immediately after recrystallization had been completed.

The characteristics of the austenite phase transformation under isothermal conditions (TTT diagrams) have been determined by dilatometry.

2.2. Industrial Trials

The verification and calibration of the models have been performed by comparing calculated values with actual bar and wire rod mill data from ILVA's plants, Piombino steel works.

On-line surface temperature measurements have been made by portable infrared pyrometers previously calibrated against a black body at the laboratory. The measurements have been carried out, with the emissivity set at 0.83, at different positions along the bar and wire rod mills, at the entry and exit side of water cooling sections (spray or tubular type) and along the Stelmor conveyor.

Specimens for austenitic microstructure evaluation were taken and water quenched at various stages of the rolling process using the mill shears. A few wire rod specimens were taken before the onset of phase transformation, by stopping the Stelmor conveyor for a few seconds and cutting off the end wraps which have been immediately water quenched.

3. Mathematical Models

The following sections describe the submodels for grain growth, static and dynamic recrystallization, transformation and structure–property relationships. These models can be used singly or linked in sequence with the output data of one model working as input data for the next model. The flow chart of the integrated mathematical models is shown in **Fig. 1**.

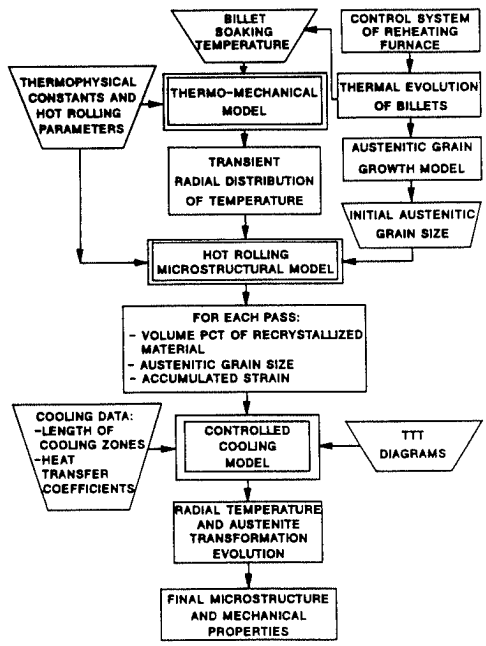

Fig. 1. Flow chart of mathematical models.

3.1. Grain Growth Model

This model is used to predict the initial austenitic grain size of those C–Mn steels which show a continuous growth.

The average size of austenitic grains ($\bar{d}_\gamma$ in μm) is given for isothermal treatments by the relationship:

$$\bar{d}_\gamma = k_1 \cdot t^{k_2} \exp(-Q_o/RT) \quad \text{.....(1)}$$

where t is the time in hours, T the absolute temperature and R the gas constant. The constants k_1, k_2, and Q_o have been identified for each steel on the basis of measurements of d_γ performed on samples subjected to different austenitization treatments (**Table 2**).

The austenitic grain size which results from a specific thermal evolution can be calculated from Eq. (1) approximating the reheating curve by a series of isothermal segments of length Δt. If in the time step t_i to $t_i + \Delta t$ the temperature increases from T_i to T_{i+1}, the increase in the austenitic grain size is calculated from the following series of equations:

$$d_{\gamma i+1} = k_1 (t^* + \Delta t)^{k_2} \exp(-Q_o/R\,T_{i+1}) \quad \text{.....(2)}$$

$$t^* = (d_{\gamma i}/(k_1 \cdot \exp(-Q_o/R\,T_{i+1}))^{1/k_2} \quad \text{.....(3)}$$

Table 2. Values of empirical coefficients.

		Low C steel ES 17	Medium C steel QC 29B	High C steel FP 69	High C steel FF 82
γ grain growth	k_1	9.1×10^{6}	*	7.9×10^{4}	4.1×10^{7}
	k_2	0.18	*	0.19	0.12
	Q_0 (KJ/mol)	126	*	69	141
Strain to peak stress (ε_p)	a	4.83×10^{-3}	2.73×10^{-3}	1.84×10^{-3}	1.84×10^{-3}
	b	0.09	0.20	0.24	0.24
Time to 50% recryst. (t_{50})	d	1.4×10^{-14}	3.2×10^{-9}	7.3×10^{-12}	4.5×10^{-5}
	e	−1.9	−1.6	−1.9	−1.0
	f	1.1	0.9	0.6	0.6
	Q_1	33.0×10^{3}	18.4×10^{3}	27.2×10^{3}	6.9×10^{3}
Recryst. volume fraction exponent (n)	g	21.3	12.2	6.2×10^{4}	6.1×10^{6}
	h	0.54	0.04	0.43	0.02
	m	−0.25	−0.10	−0.04	−0.30
	Q_2	-2.2×10^{3}	-2.6×10^{3}	-13.6×10^{3}	-18.4×10^{3}
Recryst. grain size ($d_{\gamma rex}$)	p	1 150	84	95.5	95.5
	q	−0.3	−0.6	−0.5	−0.5
	v	0.39	0.33	0.39	0.39
	Q_3	-6.5×10^{3}	-3.5×10^{3}	-3.5×10^{3}	-3.5×10^{3}

* Steel QC 29B contains Ti which was added to protect B. Its grain growth behaviour is described by the following equation:

$$d_\gamma = 95[1-\exp[-7.4\times10^{-3}\,(T-1\,133)]]$$

where d_γ is in μm and T is in K.

where t^* is the fictitious time required to reach the previous grain size $d_{\gamma i}$ at the new temperature T_{i+1}.

For microalloyed steels under reheating conditions which lead to abnormal grain growth other empirical relationships must be used.[8]

3.2. Thermomechanical Model

FEM enables the local strains, strain rates and temperature to be computed. At present only preliminary studies exist. Therefore the strain (ε) and strain rate ($\dot{\varepsilon}$) during a pass have been assumed to be the ones expected for homogeneous strain and the key variable is therefore the temperature.

The model is based on numerical integration by FDCM of the Fourier heat equation. The temperature distribution in the stock section is evaluated using an equivalent round section. Algorithms originally designed for steel plate and suitably modified to account for the different geometry are used to predict the thermomechanical cycle for a given location in the cross section of the stock. These data are used as input data for the microstructural model.

3.3. Hot Rolling Microstructural Model

The model estimates the austenitic structure developed during each pass (*i.e.* austenitic grain size of each homogeneous structure, volume fraction of recrystallized grains, amount of residual strain accumulated) as a function of the thermal and mechanical conditions (T, ε, $\dot{\varepsilon}$). The set of equations forecasting the austenitic structure is applied sequentially according to logic procedures equivalent to those proposed for flat-rolled products. In the program, structures which differ significantly one from the other are treated as separate features.[3,4]

On the basis of laboratory test results, static recovery was assumed to produce 20% softening during each pass in the roughing stage. Its effect during the finishing stage was neglected. For each homogeneous structure, a check is made to control whether the total strain (inclusive of the residual strain accumulated during previous passes ε_r) is smaller (static recrystallization) or greater (dynamic recrystallization) than the critical strain required for the onset of dynamic recystallization (ε_{dyn}). The ε_{dyn} values are calculated on the basis of the hot torsion test results using the following equations:

$$\varepsilon_p = a\cdot d_\gamma^{b}\cdot Z^{0.15} \quad \text{.....(4)}$$

$$\varepsilon_{dyn} = c\cdot\varepsilon_p \quad \text{.....(5)}$$

where $Z=\dot{\varepsilon}\cdot\exp(Q/RT)$ is the Zener–Hollomon parameter in s^{-1}, ε_p is the strain to peak stress, a and b are coefficients which depend on steel composition (Table 2) and $c=\varepsilon_{dyn}/\varepsilon_p=0.85$.

3.3.1. Static Recrystallization

Under isothermal conditions, the volume percent of material undergoing static recrystallization (R%) within a certain time t (in s) from the finish of hot deformation has been calculated with the following Avrami-type equation:

$$R\% = 100\cdot(1-\exp[-0.693(t/t_{50})^{n}]) \quad \text{.....(6)}$$

The values of the exponent "n" and of the 50% recrystallization time "t_{50}" have been calculated in terms of operating parameters T, ε and d_γ with the following equations:

$$t_{50}=d\cdot\varepsilon^{e}\cdot d_{\gamma}^{f}\cdot\exp(Q_1/T) \quad \text{.....(7)}$$

$$n=g\cdot\varepsilon^{h}\cdot d_{\gamma}^{m}\cdot\exp(Q_2/T) \quad \text{.....(8)}$$

The empirical coefficients of Eqs. (7) and (8) depend on steel composition (Table 2).

Since the strain rates applied during the finishing passes of the rolling sequence were far higher than those adopted for the hot torsion tests ($\dot{\varepsilon}=3.6$/s), the following equation, has been used to calculate the actual value of time for 50% recrystallization:

$$t_{50}(\dot{\varepsilon})=t_{50}\left(\frac{3.6}{\dot{\varepsilon}}\right)^{r} \quad \text{.....(9)}$$

where $r=0.20$–0.28.[9,10] The influence of $\dot{\varepsilon}$ is significant only for the time t_{50}.[9]

With regard to the recrystallized austenitic grain size the hot torsion results have been analyzed mathematically using an expression of the type developed for a C–Mn steel,[3] with the addition of the term $\dot{\varepsilon}^{-0.1}$ to allow for the strain rate effect[9]:

$$d_{\gamma\mathrm{rex}}=p\cdot\dot{\varepsilon}^{-0.1}\cdot\varepsilon^{q}\cdot d_{\gamma}^{v}\cdot\exp(Q_3/T) \quad \text{.....(10)}$$

where d_γ (μm) is the austenitic grain size prior to deformation and the coefficients are shown in Table 2.

In the case of partial recrystallization, the grains are smaller than those of a completely recrystallized material and are calculated from the following relationship:

$$d'_{\gamma\mathrm{rex}}=d_{\gamma\mathrm{rex}}\cdot(R\%/100)^{1/3} \quad \text{.....(11)}$$

For the fraction of material that does not recrystallize before the subsequent pass, the model calculates an effective size value which allows for elongation of the original grains and for the volume available to the work-hardened austenite[4]:

$$d_{\gamma e}=1.06\cdot d_{\gamma}\cdot(1-R\%/100)^{1/3}\cdot\exp(-\varepsilon) \quad \text{.....(12)}$$

Once recrystallization is complete, further grain growth takes place as a function of time and temperature. The relationship proposed by Sellars[10] has been used in the model.

3.3.2. Dynamic Recrystallization

The information available is very limited and the following features have consequently been adopted for formulating the model:

- The onset of dynamic recrystallization occurs when $\varepsilon>\varepsilon_{\mathrm{dyn}}$.
- The kinetics of dynamic and metadynamic recrystallization are described by the parameters t_{50} and n, calculated with the same law as established for static recrystallization. Although this hypothesis concerning dynamic recrystallization may appear arbitrary, nevertheless it can be considered as the lower limit of the actual behaviour of the material.
- The formula proposed by Senuma and Yada[11] is used for estimating the size of the dynamic recrystallized grains. This formula describes the "peculiar" growth patterns observed experimentally, *i.e.* very high growth rates during the first few seconds and subsequently very slow growth.

3.4. Controlled Cooling and Phase Transformation Model

Modern mills have special cooling sections in order to prevent grain growth and control the temperature at which air cooling starts. For these reasons a computing algorithm having a structure giving a high flexibility for simulating different operational conditions has been developed to forecast the thermal and microstructure evolution during the cooling after hot rolling.

The general Fourier heat equation, which takes into account the heat generated by the phase transformation, is integrated by finite differences, describing concurrently the evolution of the austenite during cooling. The power equations presented in Ref. 12) were used to compute the heat capacities and coefficients of thermal conductivity at different temperatures for the various microconstituents. The sharp decrease in the heat capacity of ferrite just above the Curie temperature *Tc* was not taken into account since all of the transformations started below *Tc*. The austenite transformation is determined by considering the cooling curve as a series of micro-isotherms and applying the laws governing the isothermal austenite transformation, derived by TTT diagrams, in accordance with the procedures proposed by other authors.[13,14]

Different boundary conditions can be selected for various cooling zones, each characterized by its length and rod travelling speed. The heat flow at the surface ($\dot{q}_s$) can be calculated by the following relationship:

$$\dot{q}_s=h(T_s-T_o) \quad \text{.....(13)}$$

where T_s is the surface temperature, T_o is the air or water temperature, h is a combined heat transfer coefficient which includes a heat transfer coefficient by convection heat flow (h_c) and a radiation heat transfer coefficient (h_r):

$$h=h_c+h_r \quad \text{.....(14)}$$

The values of h_c along the Stelmor conveyor have been found to be dependent primarily on the cooling air flow rate and therefore on the opening of the fan baffles. **Figure 2** shows the variation of h_c with fan opening for

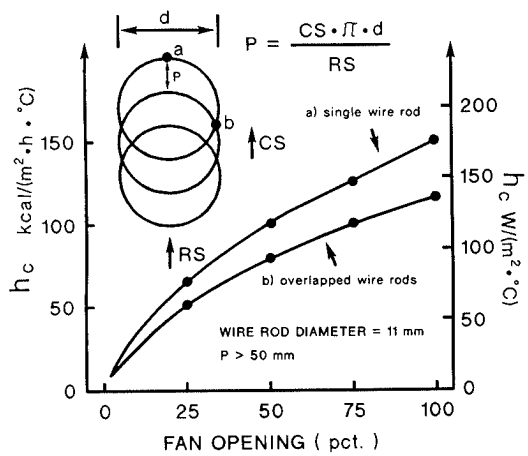

Fig. 2. Convection heat transfer coefficient (h_c) on the Stelmor conveyor calculated using surface temperature measurements. *P* is a measure of wire rod overlapping (see graph inset).

specific working conditions. Wire rods which are not overlapped show a heat transfer coefficient, h, about 20% higher.

The onset of phase transformation is calculated on the basis of the Scheil's hypothesis.[13,14] No difference is made between ferrite and pearlite. However, the volume fraction formed between Bs and Ms is identified as consisting of bainite and the volume fraction formed below Ms as consisting of martensite.

The fraction of austenite which transforms to ferrite and pearlite or to bainite is calculated according to Avrami's law[15]:

$$V_i = 1 - \exp\left[-b_i \cdot \left(\frac{d_{\gamma TTT}}{d_\gamma} \right)^2 \cdot t^{n_i} \right] \quad \text{.....(15)}$$

in which V_i represents the fraction of austenite that transforms at the temperature T_i. The coefficients b_i and n_i vary with temperature and are derived from the TTT diagram determined for a grain size $d_{\gamma TTT}$. The model follows the procedure proposed by Agarwal and Brimacombe[13] where each TTT curve is approximated to a series of linear segments in logarithmic scale to simplify calculation of coefficients b_i and n_i. The fraction of austenite transformed at temperature T_i above Ms is calculated by solving Eq. (15) at time t_i; this time value is equal to the sum of the time interval Δt (during which the temperature value is T_i) and of the "equivalent" time required for the transformation at temperature T_i of an amount of austenite equal to that transformed during the entire previous time.

For temperatures below Ms, the fraction of austenite that transforms to martensite is calculated with the equation proposed by Koistinen and Marburger[14]

$$V_\gamma = (1 - \sum V_i)[1 - \exp[-0.0110(\mathrm{Ms} - T)]] \quad \text{...(16)}$$

where Ms is the martensite start temperature and $(1 - \sum V_i)$ is the fraction of untransformed austenite.

Using a steel of similar composition to the eutectoid steels employed in the present investigation, Iyer *et al.*[16] calculated the interlamellar spacing of pearlite using:

$$s\,(\mathrm{mm}) = \frac{1.8 \cdot 10^{-2}}{\Delta T_E\,(^\circ\mathrm{C})} \quad \text{.....(17)}$$

The same formula was adopted in this work, with the average undercooling relative to A_{e1} (ΔT_E) being taken as the average between the maximum value at the start of transformation and the minimum value at the peak of recalescence.

The dependence of ferrite grain size (d_α) on austenite grain size and average cooling rate (C_R) in steels having a ferrite–pearlite microstructure was found to be:

$$d_\alpha = A d_\gamma^{0.4} (1 - \exp(0.075 d_\gamma)) C_R^{-0.14} \quad \text{.....(18)}$$

where the constant A varies with composition, d_α and d_γ are expressed in μm and C_R in °C/min. Since the three steels considered had comparable calculated Ar_3 temperatures,[17] the effect of their compositional differences on d_α was neglected on the assumption that C, Mn and Si act on d_α mainly through their effect on Ar_3.

3.5. Mechanical Properties–Structure Relationships

Microstructural parameters estimated by the models are converted to mechanical property information using various empirical regression formulas.

The hardness of each phase is calculated from the chemical composition according to the expressions developed by Creusot–Loire.[18] The total hardness is calculated using a linear mixture law.

The ductility of pearlitic steels is mainly controlled by the austenitic grain size d_γ.

On the basis of experimental data the following equation has been obtained for the reduction of area (Z) of eutectoid steels:

$$Z(\%) = 25.2 - 0.36 \cdot 10^6 t + 2.48 d_\gamma^{-1/2} \quad \text{.....(19)}$$

where d_γ and t (cementite thickness) are expressed in mm. The cementite thickness t is a function of carbon content and interlamellar spacing of pearlite.

The ultimate tensile strength (UTS) of pearlitic steels depends on the interlamellar spacing and was calculated according to the equations proposed by Gladman.[19,20]

4. Validation of Models

A set of equations with empirically determined coefficients were worked out to relate the heat transfer coefficient to the operating conditions of the mill. An example of the predicted temperature profiles through a bar mill compared with experimental surface temperatures is shown in **Fig. 3**. All the calculated values were found to be in good agreement with the corresponding measured values (relative differences of less than 5%).

Figure 4 shows a comparison between the calculated and measured surface temperature values of high-carbon and boron steel wire rods on the Stelmor conveyor under specified operating conditions.

The predictions made by the model are in very good agreement with the experimental values, since the deviations match the spread of the experimental data ($|\Delta T| < 20^\circ$C).

Figure 5 shows a comparison between calculated and measured mean austenite grain sizes. The predictions are fairly accurate (standard deviation 10%) considering that they cover 26 rods of different steels, rolled to different diameters, investigated at two different points (centre

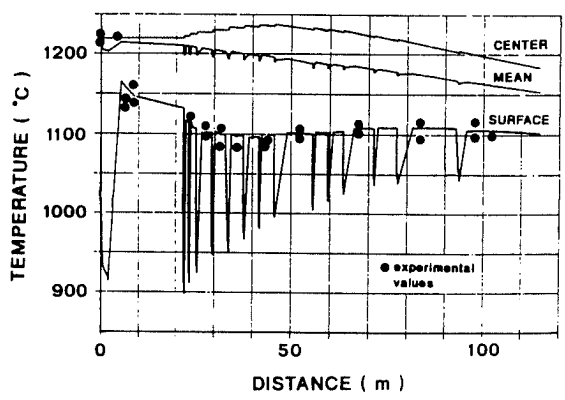

Fig. 3. Temperature profile during hot rolling of 42 mm diameter bars.

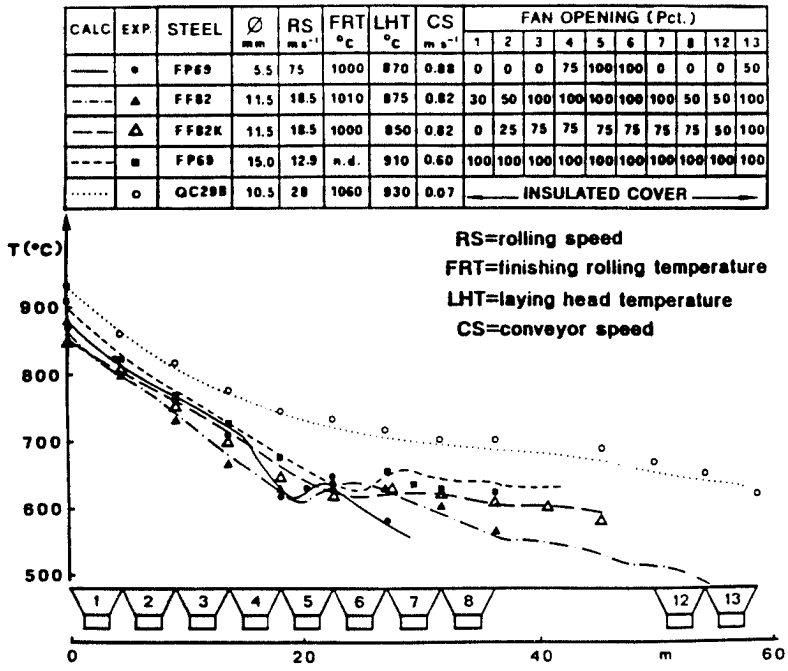

Fig. 4.
Comparison between calculated and measured surface temperatures of wire rods during controlled cooling.

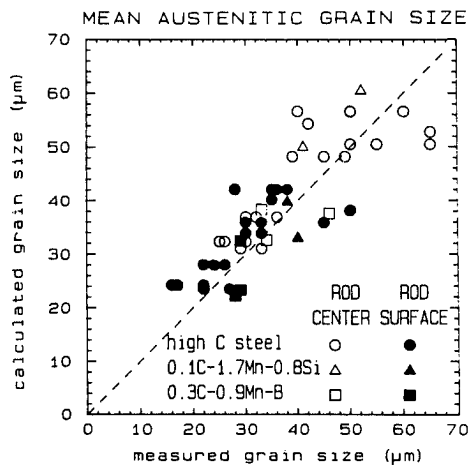

Fig. 5. Comparison between calculated and measured mean austenitic grain sizes in full-scale trials.

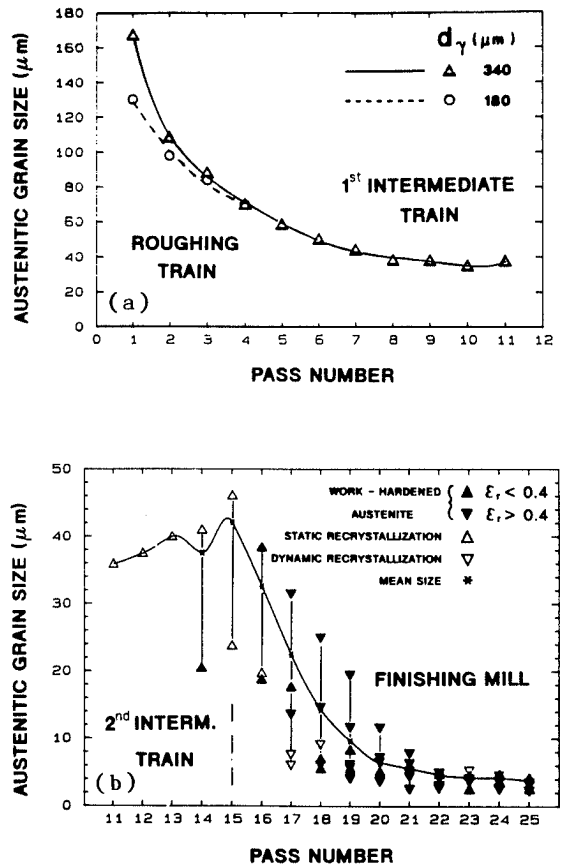

Fig. 6. Predicted evolution of austenitic grain size: (a) roughing, (b) finishing.

and surface).

An example of the predicted austenite grain size evolution during rolling is shown in **Fig. 6**. During the roughing stage (Fig. 6(a)), the interpass times are sufficiently long to allow for complete recrystallization with progressive grain refining. During finishing (Fig. 6(b)), only partial recrystallization occurs despite the very rapid kinetics, since the interpass times become progressively shorter ($t<0.07$ sec). Refining of the austenitic structure during the finishing stage is clearly brought on by the occurrence of partial static recrystallization processes, followed by dynamic recrystallization of the strongly work-hardened fraction of material. This leads to the formation of a heterogeneous structure (even if the grains are initially all of the same size) within a few seconds after the last pass, owing to the high growth rate of the dynamically recrystallized grains.

Detailed analysis of the structure of 11 and 5.5 mm diameter rod specimens, quenched 15–20 sec after the end of rolling, revealed that the measured grain size distributions followed a bimodal pattern as predicted by the model (**Table 3**).

In order to test the reliability of the model more radically (especially with regard to the kinetics associated with the very high growth rates of dynamically recrystallized grains), mill conditions were set up for blocking the rod in the water box facing the exit of the

finishing stand. In this way, it was possible to freeze the austenitic structure of a high carbon steel within 0.5 sec from the end of rolling. Metallographic examination of longitudinal and transversal sections of the rod revealed the presence of a fully recrystallized structure consisting of two different grain populations as predicted by the recrystallization model (Table 3).

5. Industrial Applications

The ability of the proposed "complete model" in simulating the industrial processes and its potential usefulness in designing and solving problems have been demonstrated by significant examples of calculation of hot rolling and controlled cooling of wire rods and bars.

5.1. Hot Rolling

Examples of the effect of hot rolling practice on the formation of heterogeneous austenitic structures have been already discussed. Local heterogeneity increases with billet temperature and becomes progressively more pronounced from the surface to the centre of the rod (**Table 4**).

The model is also able to predict the variation of the mean austenite grain size along the stock diameter due to the thermal gradient. **Figure 7** shows the comparison of experimental and calculated mean grain sizes in a 17 mm diameter rod. The agreement is good despite the fact that the strain variation is not considered.

The positive effect of reducing the billet soaking temperature and the rolling speed for the refinement of austenitic grains of 21 mm diameter bars is shown in **Table 5**. A reduction in austenitic grain size of about 30% can be obtained.

5.2. Controlled Cooling of Wire Rods

The influence of wire rod diameter, cooling practices and axial segregation on microstructure and strength has

Table 3. Comparison between calculated and measured data relative to heterogeneous austenitic structures in high-carbon steel rods.

Wire rod diameters (mm)	Time after end of rolling (s)	Experimental values Volume (%)	Experimental values d_γ (μm)	Calculated values Volume (%)	Calculated values d_γ (μm)
5.5	17	79.7	23.9	68.4	31.6
		20.3	11.4	31.6	10.9
11.0	22	51.2	36.4	71.8	31.9
		48.8	18.7	28.2	17.7
5.5	0.5	59.0	21.8	58.8	20.2
		41.0	12.8	41.2	10.6

Table 4. Calculated austenitic grain size heterogeneity (σ) of 5.5 mm rods for different billet soaking temperature.

	Rod surface		Rod center	
Billet soaking temperature (°C)	1 140	1 190	1 140	1 190
$\bar{d}_\gamma$ (μm)	17.9	22.1	28.5	31.1
σ (μm)	7.6	9.1	11.9	13.2

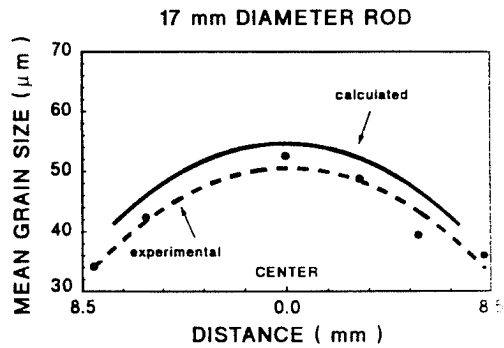

Fig. 7. Comparison of experimental and calculated austenitic grain size profile along the rod diameter (high-carbon steel).

Table 5. Predicted effect of soaking temperature and rolling speed on austenitic grain size of 21 mm diameter bars.

Soaking temperature (°C)	Rolling speed (m/s)	Mean grain size (μm) Surface	Mean grain size (μm) Center
1 200	12	68.3	78.4
1 160	9	48.5	58.8

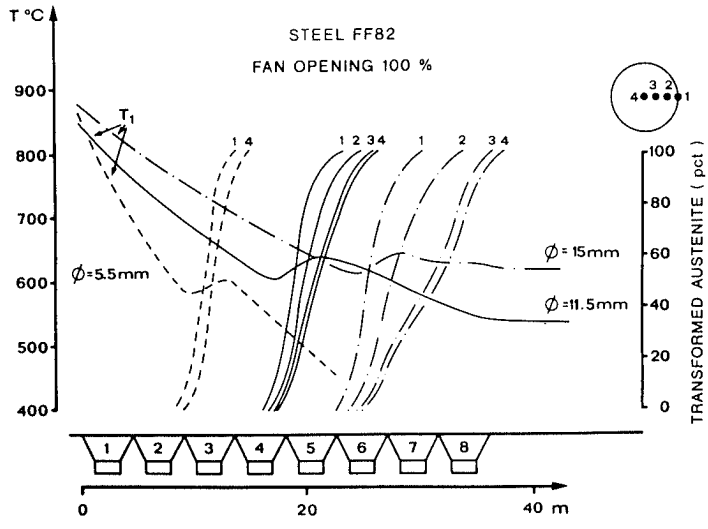

Fig. 8.
Predicted effects of wire rod diameter on local temperature and fraction of transformed austenite.

been investigated.

5.2.1. Effect of Wire-rod Diameter

For equal cooling conditions (all fans turned on), an increase in rod diameter from 5.5 to 15 mm causes an increase of the estimated mean pearlite formation temperature from 610 to 650°C (**Fig. 8**). This in turn causes an increase of calculated lamellar spacing from $s=150$ nm to $s=230$ nm and corresponding reduction in mechanical strength (ΔUTS $=-55$ MPa).

5.2.2. Effect of Cooling Practices

The models have been used in a specific application aimed to reduce the cooling rate down to the point where the strength of the wire rod could still be guaranteed to be greater than 1 030 MPa. The reduction of the cooling rate was planned to prevent the formation of brittle structures in the segregation zones of 5.5 mm diameter rods (see Sec. 5.2.3). **Figure 9** shows the calculated temperature and strength values, relative to the original situation and to the new practice singled out with the model, compared with the experimental data. These results confirm the model capacity to yield reliable information for selecting the optimum on-line cooling practice.

Another practical problem in wire rod mill is to avoid the formation of bainite or martensite in steels with high hardenability such as boron steels for fasteners. An insulated cover and low conveyor speeds are usually adopted to give very dense loops and thus low cooling rates.

In **Fig. 10** the effects of laying head temperature (LHT) and conveyor speed (CS) on the temperature profile and transformed austenite fraction are shown for 10.5 mm diameter rods.

The phase transformation is not completed in the insulated zone and the formation of acicular microstructure cannot be avoided when critical values for LHT and CS are reached.

If low LHT values are difficult to be obtained the simulation suggests that it is convenient to shift the insulating cover a few meters to favour a rapid temperature decrease up to the start of phase transformation.

5.2.3. Central Segregation Effects

Formation of bainite and martensite, which give rise to problems during drawing, is favoured by high cooling rates and by the increase of local hardenability due to segregation of elements such as C and Mn at the

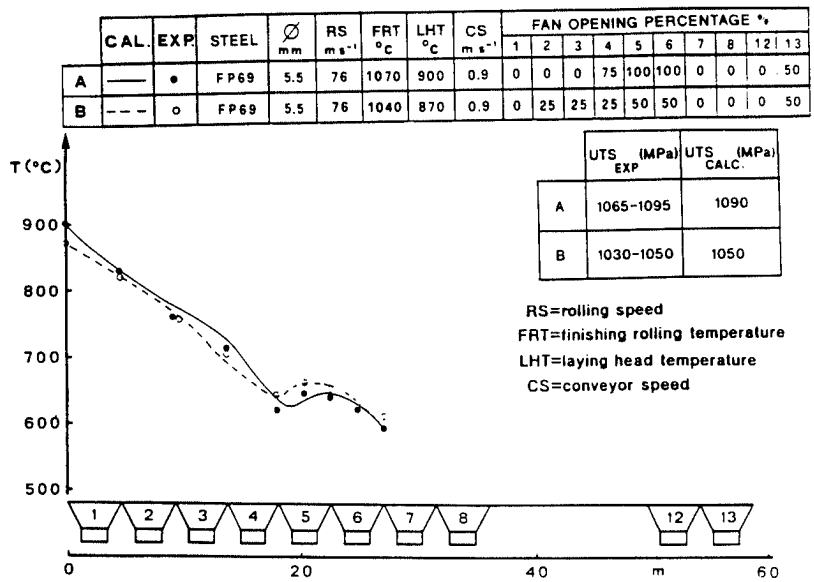

Fig. 9.
Predicted temperature profile of 5.5 mm diameter high-carbon steel wire rods along Stelmor conveyor.

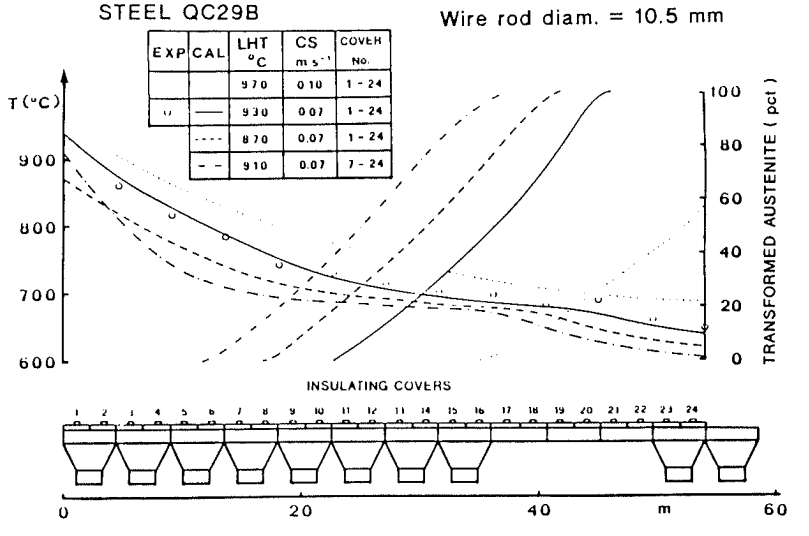

Fig. 10.
Temperature and austenite evolution during retarded cooling on the Stelmor conveyor for boron steel wire rod.

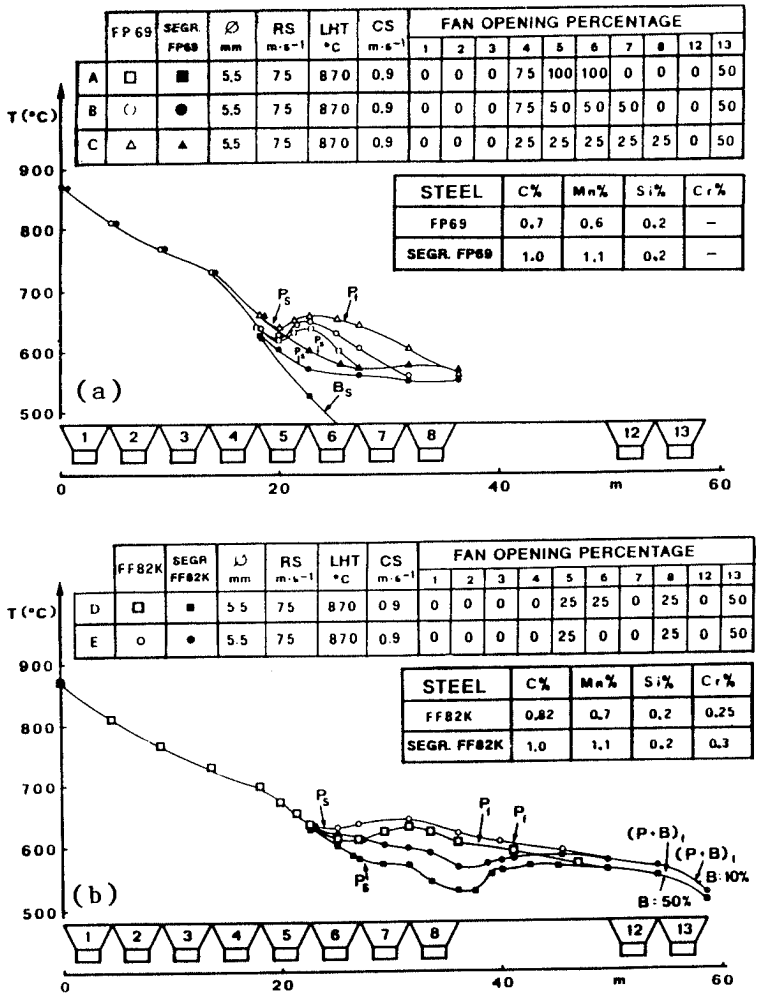

Fig. 11.
Predicted effect of central segregation and cooling on temperature profile and final microstructure of 5.5 mm diameter high-carbon steel wire rods.

centreline of the wire rod. **Figure 11** shows the model results for 5.5 mm diameter rods which are more prone to the formation of undesirable phases since they can be cooled rapidly. The effect of segregation on phase transformation kinetics was taken into account by shifting the start and end of transformation according to available information[21] on the influence of chemical composition derived from TTT diagrams.

To prevent the formation of bainite and/or martensite it is necessary to modify the cooling practice, starting from the point on the Stelmor conveyor where pearlite starts to form on the rod surface. From that point onwards, the airflow rate of the fans should be reduced drastically for a conveyor length sufficient to ensure the transformation to pearlite of the austenite in the central segregation zone (Fig. 11(a)).

In the case of a more hardenable steel (Fig. 11(b)), it is necessary to shut down two fans at the onset of pearlite transformation. This operation reduces drastically the formation of bainite, which otherwise would amount to over 10%. Setting the baffles of fan No. 8 to a 25% opening contributes to keeping the temperature of the pearlite transformation within medium values (640°C), thereby avoiding the formation of coarse pearlite.

5.3. Bar Cooling

Very rapid cooling systems are required to reduce the stock temperature for controlling grain growth after hot rolling as the usual distances between finishing roll and cooling bed are rather small. However, if severe cooling occurs temperatures can reach values lower than 400°C and martensite formation could result at the surface.

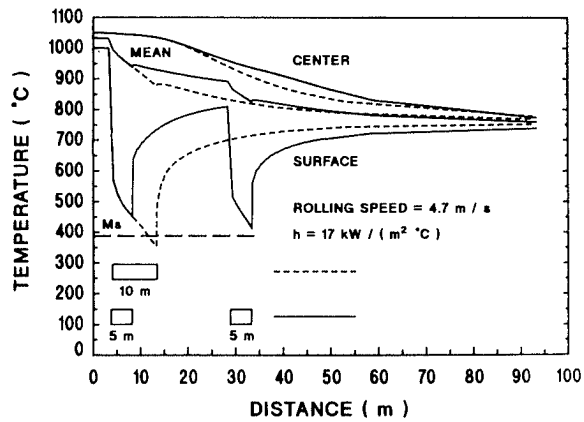

Fig. 12. Predicted effect of cooling system layout on temperature profile of 32 mm diameter bar.

In **Fig. 12** the effect of the cooling system layout (heat transfer coefficient of 17 kW/(m² °C) on temperature profiles of 32 mm diameter bar is shown.

Two cooling sections, 5 m long each, instead of one 10 m long cooling zone, succeed in achieving lower stock temperatures without inadmissible undercooling of the bar surface, avoiding martensite formation.

6. Conclusions

A system of mutually integrated mathematical models has been applied for investigating the relationships between process variables and the thermal and microstructural homogeneity of wire rods and bars.

The presence of thermal gradients along the diameter of the rod and the effect of different recrystallization mechanisms can lead to the formation of heterogeneous austenitic structures.

Using the model, it has been possible to quantify the effects of rod diameter and cooling practices on the microstructure and temperature profile along the Stelmor conveyor.

The degree to which bar surfaces can be cooled by water tube systems avoiding martensite formation has been determined.

Among the practical objectives already achieved, or which can be achieved in the short term by applying the microstructural mathematical model, are:

- optimization of the hot rolling and cooling practices for the materials currently in production;
- identification of controlled cooling conditions for new steels, with a consequent reduction of industrial experiments;
- prediction of the improvements obtainable trough plant modifications (*e.g.* introduction of additional cooling systems in the mill to reduce finish rolling temperature);
- identification of simplified models for on-line use.

REFERENCES

1) Proc. Int. Conf. on Physical Metallurgy of Thermomechanical Processing of Steels and Other Metals (THERMEC-88), ISIJ, Tokyo, (1988).
2) Proc. Int. Symp. Mathematical Modelling of Hot Rolling of Steel, ed. by S. Yue, CIM, Hamilton, Ontario, Canada, (1990).
3) E. Anelli *et al.*: Proc. of 7th Int. Conf. on Strength of Metals and Alloys, ICSMA 7, ed. by H. J. McQueen *et al.*, Pergamon Press, New York, (1985), 1031.
4) E. Anelli *et al.*: Proc. of Int. Conf. on HSLA Steels '85, ed. by J. M. Gray *et al.*, ASM, Ohio, (1985), 683.
5) E. Amici *et al.*: Proc. Numiform 89, July 1989, Fort Collins, ed. by E. G. Thompson *et al.*, Balkema, Rotterdam, (1989), 293.
6) N. Kapaj *et al.*: *Eng. Comput.*, **5** (1988), No. 2, 151.
7) P. Choquet *et al.*: THERMEC-88, ISIJ, Tokyo, (1988), 729.
8) E. Anelli, M. Paolicchi and G. Quintiliani: Communication presented at MatTech '90, June 1990, Helsinki, Finland, (1990).
9) P. Choquet *et al.*: Proc. of 7th Int. Conf. on Strength of Metals and Alloys, ed. by H. J. McQueen *et al.*, Montreal, Pergamon Press, New York, (1985), 1025.
10) C. M. Sellars: 7th RISØ Int. Symp. on Metallurgy and Mat. Sci, ed. by N. Hansem *et al.*, (1986), 167.
11) T. Senuma and H. Yada: 7th RISØ Int. Symp. on Metallurgy and Materials Science, ed. by N. Hansen *et al.*, (1986), 547.
12) B. Hildenwall and T. Ericsson; Proc. Int. Symp. on Hardenability concepts with applications to steel, ed. by D. V. Doane and J. S. Kirkaldy, TMS AIME, Penn., (1978), 579.
13) P. K. Agarwal and J. K. Brimacombe: *Metall Trans. B*, **12B** (1981), 121.
14) S. Denis, S. Sjöström and A. Simon: *Metall. Trans. A*, **18A** (1987), 1203.
15) I. Tamura: *Trans. Iron Steel Inst. Jpn.*, **27** (1987), 763.
16) J. Iyer, J. K. Brimacombe and E. B. Hawbolt: Prof. Conf. on Mechanical Working and Steel Processing XXII, Chicago 1984, ISS/AIME, Penn, (1985), 47.
17) C. Ouchi *et al.*: *Trans. Iron Steel Inst. Jpn.*, **33** (1982), 214.
18) Ph. Maynier, B. Jungmann and J. Dollet: Hardenability Concepts with Applications to Steel, ed. by D. V. Doane and J. S. Kirkaldy, AIME, Chicago, (1978), 518.
19) T. Gladman, I. D. McIvor and F. B. Pickering: *J. Iron Steel Inst.*, **210** (1972), 916.
20) T. Gladman: *Ironmaking Steelmaking*, **16** (1989), 241.
21) Y. I. Park, F. B. Fletcher: *J. Heat Treat.*, **4**, (1986), No. 3, 247.